ROYAL SOCIETY OF CHEMISTRY

COMMUNICATION

Check for updates

Cephalopod chromatophores contain photosensitizing nanostructures that may facilitate light sensing and signaling in the skin†

Taehwan Kim, Duncan Q. Bower and Leila F. Deravi [iD] *

Cephalopods can sense and respond to changes in their environment using combinations of pigments, proteins, and/or nanostructures which are sequestered in the stratified optical organs of their dermal tissue. Of these organs, the chromatophore functions as a dynamic optical filter that imparts rapid and adaptive changes to the color and patterns presented in cephalopod skin. Chromatophores contain pigmented granules, but there is very little information available on whether their function extends beyond pigmentation. We examine granule performance within a photovoltaic cell and investigate their light sensing properties. Upon exposure to solar simulated light, photoexcited charge transfer is observed in devices containing the granules, where a photoconversion efficiency up to 0.81 ± 0.14% is recorded. This finding is the first to suggest that these biomaterials function as more than simple colorants; they may also be involved in light sensing and transduction to support adaptive camouflage.

Introduction

Cephalopod camouflage is enabled by combinations of light scattering, absorption, reflection, and refraction[1–4] through a network of chromatic and emissive units controlled directly and indirectly *via* the central nervous system.[5,6] There are multiple dermal organs that participate in regulating body color. These include chromatophores layered on top of reflecting cells like iridophores. Chromatophores are pigmented organs presented as yellow, red, and brown/black colors, where the primary pigmentary component is the nanostructured granules containing xanthommatin or decarboxylated xanthommatin.[7,8] These granules are generally spherical with diameters ranging from 200 to 800 nm depending on color. Contraction and relaxation of radial muscle fibers surrounding

the central pigment sac of the chromatophore is correlated with its neuronal innervation, suggesting neuromuscular control of the dynamic structures. During an actuation cycle, the pigment sac can expand up to 10 times its original size and can operate synchronously with hundreds of adjacent chromatophores to present complex patterns and shapes across multiple spatial scales.[4,9] While our understanding of the molecular contributions enabling color change and pattern formation enabled by cephalopod chromatophores is evolving, mechanisms underlying signal transduction within a single chromatophore and across neighboring chromatophores are not yet understood. One intriguing potential influence on the creation of color patterns on the body is the light in the environment. In general, body patterning in cephalopods depends on communication between three major components: the eyes, the central nervous system (CNS), and the skin.[10,11] Previous studies reveal that squid and octopus chromatophores in dissociated skin respond directly to light exposure. The expression of opsin mRNAs in cuttlefish skin may be linked to this light sensitivity, as r-opsin based phototransduction genes have been observed in both the eyes and skin of some cephalopods.[12,13] Ramirez *et al.* formalized this behavior in *Octopus bimaculoides* skin as "light-activated chromatophore expansion," when they found that the chromatophore seems to directly sense illuminated light, with maximal responses achieved and sustained upon continuous blue (480 nm) light exposure.[14] This suggests that cephalopod skin may be intrinsically sensitive to light; however, it is still unclear how light sensitivity connects to the electromechanical function of the chromatophore required for global color change.

It is well known that cephalopod chromatophores are sensitive to electrical stimulation. In one example, electrophysiological studies on semi-intact *Sepioteuthis lessoniana* demonstrated that chromatophore expansion and retraction synchronized with quasi-sympathetic wave-like patterns at oscillating frequencies below 1.5 Hz.[15] Even though these patterns were generated by stimulating CNS motor neurons, the remarkable large-scale resonance of chromatophores

Department of Chemistry and Chemical Biology, Northeastern University, Boston, MA 02115, USA. E-mail: l.deravi@northeastern.edu

suggests electrical communication between chromatocytes that is controlled by the CNS. Despite this correlation, it is uncertain how electrical signal propagates across and through a single chromatophore to reach a neighboring unit. The possibility of electrical amplification within the chromatophore could address this. For this to be true, there must be electron transfer within/throughout the granules of the chromatophore. By definition, the inclusion of pigments in a biological system creates opportunities for light interaction, thus leading to a higher probability of photonic energy.[16] In conjunction with a putative protein–pigment complex interaction presupposed in each granule,[8] this photonic energy could stimulate electron transfer, and by extension, amplification and signal transduction across the chromatophore organ for camouflage.[17,18] To test this hypothesis, we examined the light-sensitizing function of pigment granules extracted and purified from squid chromatophores assembled as part of a photovoltaic cell. Inspired by the design of dye-sensitized solar cells (DSSCs) which produce electrical energy through charge injection into the semiconductor from a highly absorptive layer of photosensitive dyes *via* an interstitial electrolyte,[19–21] we used isolated chromatophore granules as photosensitizers in these cells and interrogated their capacity to transduce light into energy. To accomplish this goal, we first defined the energy bandgaps of isolated pigment granules and their component parts using combinations of UV-vis absorption spectra and energy level estimation using electrochemical analysis. Next, photoconversion efficiency (PCE) of assembled devices containing granules were measured, where we observed PCE values up to $0.81 \pm 0.14\%$ with a corresponding increase of photocurrent generation of 2.5 ± 0.15 mA cm^{-2} at the highest granule loading densities. When compared to the control (no granules), synthetic pigment, and soluble pigment extracted from the granules, we found that the granules consistently outperformed the other conditions, suggesting an important structural and functional contribution to signal transduction unique to the chromatophore granules only.

Methods

Granule extraction

Granules were extracted from chromatophores from deceased adult *Doryteuthis pealeii*, which were received from the Marine Resources Center (MBL, Woods Hole, MA). Because ethics approval is not required for work on cephalopods in the United States, no Institutional Animal Care and Use Committee approval was needed for this work. Still, the authors attest to conducting all experiments with caution and care, where only the minimal number of animals were used in the studies. To isolate the granules, the epidermal skin layer of the deceased *D. pealeii* was first carefully removed, and the intact chromatophore layer was treated with a 6 mg mL^{-1} solution of collagenase (*Clostridium histolyticum*, Sigma-Aldrich) and 1 mg mL^{-1} of papain (Thermo Scientific) solution similar to past reports.[7,8] Granules were isolated from the tissue following a sequence of

sonication, washing, and centrifugation (5 min at 18 k rcf) steps and were stored at 4 °C until use.

Pigment extraction from the granule

The purified, extracted granules were treated with 500 μL of 5% v/v hydrochloric acid (Sigma-Aldrich) in methanol (Sigma-Aldrich). This suspension was vortexed, sonicated, and centrifuged. After which, the visibly pigmented supernatant was collected, and the transparent pellet was discarded.

Xa synthesis

Xa was synthesized similar to past reports, where 4 mg of 3-hydroxy-DL-kynurenine (3OHK) (Sigma-Aldrich) was first dissolved in 1 mL DI water neutralized in sodium hydroxide (Sigma-Aldrich) containing 16.5 g of potassium ferricyanide (Thermo Scientific) and stirred at room temperature. After 90 min, Xa was precipitated from the reaction using concentrated acid hydrochloric acid (Sigma-Aldrich) and washed with water until further use.

Preparation for TiO$_2$ paste

7.5 g of titanium dioxide (TiO$_2$, P25, Degussa) was mixed in 10% v/v acetylacetone (Fisher) to create the paste used in the photovoltaic cells. This mixture was stirred for three days, and finally 2.5% v/v Triton X-100 (Sigma-Aldrich) was added to the well-dispersed colloidal solution before use.

Fabrication and testing of DSSCs

DSSCs were assembled using a layer-by-layer approach (Fig. 1). The photoanode was prepared using a doctor blade method to create a thin film of TiO$_2$ paste which produced a film thickness of ~ 23 μm on an FTO coated glass substrate (MSE supplies, 7–8 Ω sq^{-1}, FTO TEC 7 coated glass substrate). The films were then annealed at 450 °C for 60 min in air. For sensitization, films were soaked in different concentrations of granules (or synthetic Xa and extracted pigments) in 90% v/v acetonitrile (Fisher) overnight at room temperature in a shaking bath. The samples were than rinsed with acetonitrile and dried in air to remove the excess dyes. Devices were assembled with a counter electrode that was prepared on a FTO glass substrate coated with 0.01 mol L^{-1} of chloroplatinic acid (H$_2$PtCl$_6$, Sigma-Aldrich) in isopropanol (Fisher) and annealed at 350 °C for 30 min in air. Finally, the electrolyte containing 4 mL propylene carbonate (Sigma-Aldrich) by adding 0.5 mol L^{-1} lithium iodide (Sigma-Aldrich), 0.05 mol L^{-1} iodine (Sigma-Aldrich), 0.5 mol L^{-1} 1-butyl-3-methylimidazolium iodide (Sigma-Aldrich), and 0.5 mol L^{-1} 4-*tert*-butylpyridine (Fisher) was added, and the device was sealed with an adhesive.

Morphology and thickness studies

Surface and cross-sectional analyses were conducted using scanning electron microscopy (Hitachi S-4800 FE-SEM).

Optical measurements

The UV-vis absorption spectra of the extracted granules (or extracted pigments and synthetic Xa) in solution and deposited

This journal is © The Royal Society of Chemistry 2025

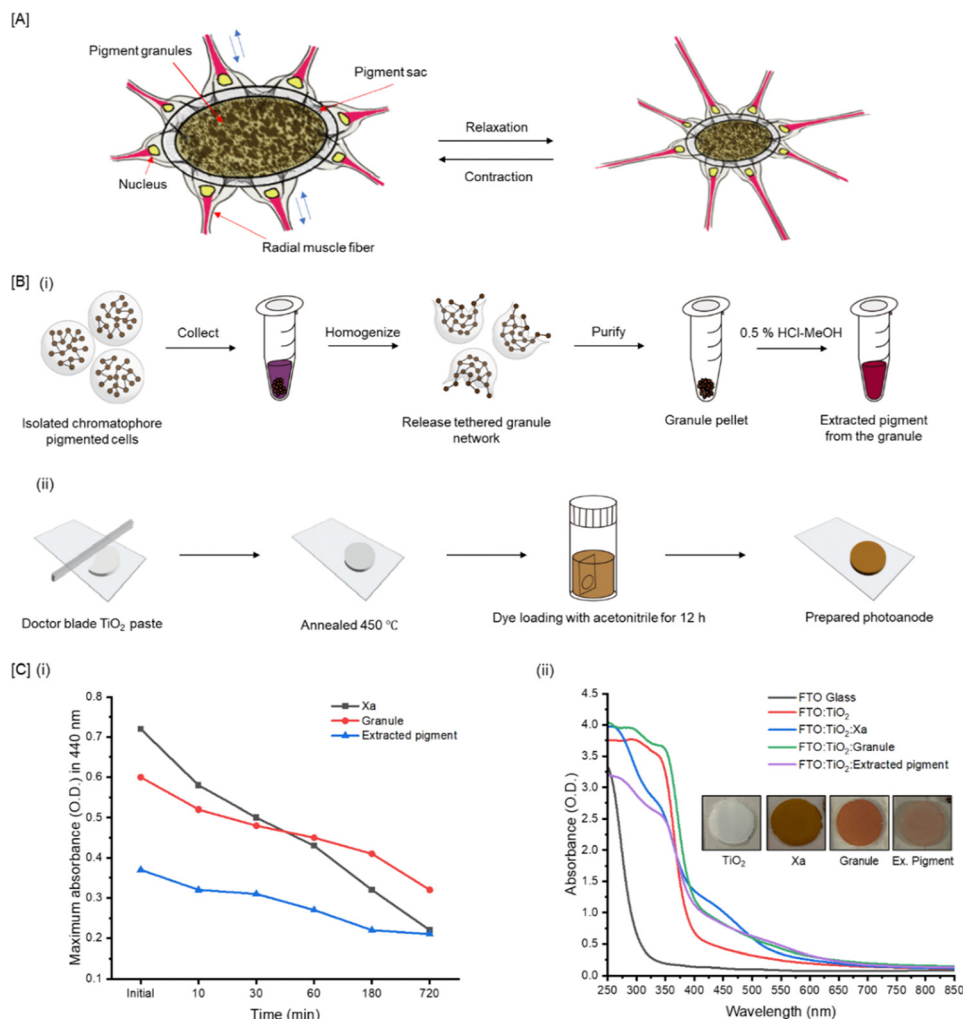*J. Mater. Chem. C*, 2025, **13**, 1138–1145 | **1139**

Fig. 1 Fabrication and characterization process for the chromatophore granule-based DSSCs. (A) Illustration of chromatophore contraction and relaxation and the associated parts of the organ. The nanostructured granules are in the central pigment sacculus. (B) Overview of the (i) extraction process of chromatophore granules from the isolated chromatocytes and extraction of the pigment from within the granules and the (ii) procedure for preparing the granule-based DSSCs with a final circular active area of 0.35 cm^2. (C) Tracking the changes of the absorbance spectra of each "dye" (62.5 mg mL^{-1}) during the photoanode incubation step, including (i) changes to the soluble dye content within the soaking medium over the 12 h (720 min) incubation period and (ii) the absorption spectra of granule, extracted pigment, and synthetic Xa loaded TiO$_2$ films after the 12 h incubation is completed. Photos of each film are presented in the inset.

as thin films were collected using UV-vis spectroscopy (Thermo Scientific, Evolution 220 UV-visible spectrophotometer).

Electrochemical measurements

Electrochemical experiments were conducted using a Gamry Interface 1000B potentiostat with a three-electrode cell, which included carbon glassy electrode as the working electrode, a platinum wire as the counter electrode, and Ag/AgCl (with saturated KCl) as the reference electrode. The current–voltage (I–V) measurements were reported using 3 mL of 0.25 mg mL^{-1} of granules (or extracted pigments and synthetic Xa) in 0.1 mol L^{-1} phosphate buffer as the electrolyte (pH 7). The potential range was −0.2 to 0.2 V using a 50 mV s^{-1} scan rate. Electron transport processes of prepared cells were collected by

electrochemical impedance spectroscopy (EIS) with same potentiostat in dark and illuminated light conditions across 10 000 Hz to 0.01 Hz and an oscillating voltage of 10 mV in two-electrode configuration.

HOMO/LUMO calculation

To determine the relevant energy levels of HOMO and LUMO for each sensitizer, the oxidation and reduction peaks from CV curves, following eqn (1) and (2) were used.[22] Here, E_g is determined from the generated Tauc plot.

$$E_{HOMO} = -e(E_{oxidation\ vs.\ NHE} + 4.75) \text{ or } -e(E_{reduction\ vs.\ NHE} + 4.75) \tag{1}$$

$$E_{LUMO} = E_g + E_{HOMO} \tag{2}$$

1140 | J. Mater. Chem. C, 2025, 13, 1138–1145

This journal is © The Royal Society of Chemistry 2025

Photovoltaic measurements

The current density–voltage (*J–V*) characteristics of the cells were measured with a source measure unit (SMU, Ossila Xtralien X200) under exposure of 1 sun (100 mW cm^{-2}) illuminated intensity. A solar simulator (Oriel LCS-100, solar simulator, Xe lamp) was employed as the light source. The incident light intensity was calibrated with a solar power meter (Extech Instruments). The photovoltaic parameters were measured immediately after exposing the prepared cells to light.

Results and discussion

Optical properties

Cephalopod chromatophores are complex, multicomponent organs (Fig. 1A). We hypothesize that granules within the central pigment sac are active components in light sensing/signaling for camouflage. To test this hypothesis, we first isolated granules and their component parts (Fig. 1B(i)) and incorporated them onto photoanodes made of a custom formulated TiO$_2$ paste of FTO glass (Fig. 1B(ii)). To maximize the loading density of the chromatophore-based colorants on the TiO$_2$ semiconductor, we first varied the concentration of each additive to enrich color transfer. The primary colorants of the granules are xanthomatin (Xa) and its decarboxylated form (DC–Xa) which have maximum absorption in the visible region centered around 435–485 nm.[7,23] As expected, extracted granules and pigments isolated from the granules have similar absorption spectra compared to synthetic Xa, where loading density is dependent on concentration and incubation time (Fig. 1C(i) and Fig. S1, ESI†). When monitored over 720 min (12 h) of incubation in acetonitrile, we observed that 46.6%, 69.4%, and 43.2% of the total granules, synthetic Xa, and extracted pigment respectively were transferred to the photoanode, as no dye was adhered to the vessel (Fig. 1C(i)). Of the conditions tested, synthetic Xa exhibited the fastest adsorption process, which we believe is due to its binding affinity to the oxide film.[24] The granules and pigment extracted from the granules were slower likely due to their complex composition, which includes proteins[8] and, in the case of the granules, nanostructures that were ∼20× greater than the TiO$_2$ used in the paste (Fig. S2, ESI†). Despite this observation, all films produced rich visible colors compared to the TiO$_2$ control (Fig. 1C(ii)).

Based on the collected UV-vis spectra of prepared dye loaded TiO$_2$ films, a Tauc plot[25] was constructed to extrapolate the bandgap of the respective materials. These were estimated at 3.19, 3.16, and 3.15 eV for the extracted granule, synthetic Xa, and extracted pigment, respectively (Fig. 2A and Fig. S3A, ESI†). These values were compared to the extrapolated energy bandgap of the TiO$_2$ used in our photoanode (3.27 eV), which was also in good agreement with previous reports for TiO$_2$[26]
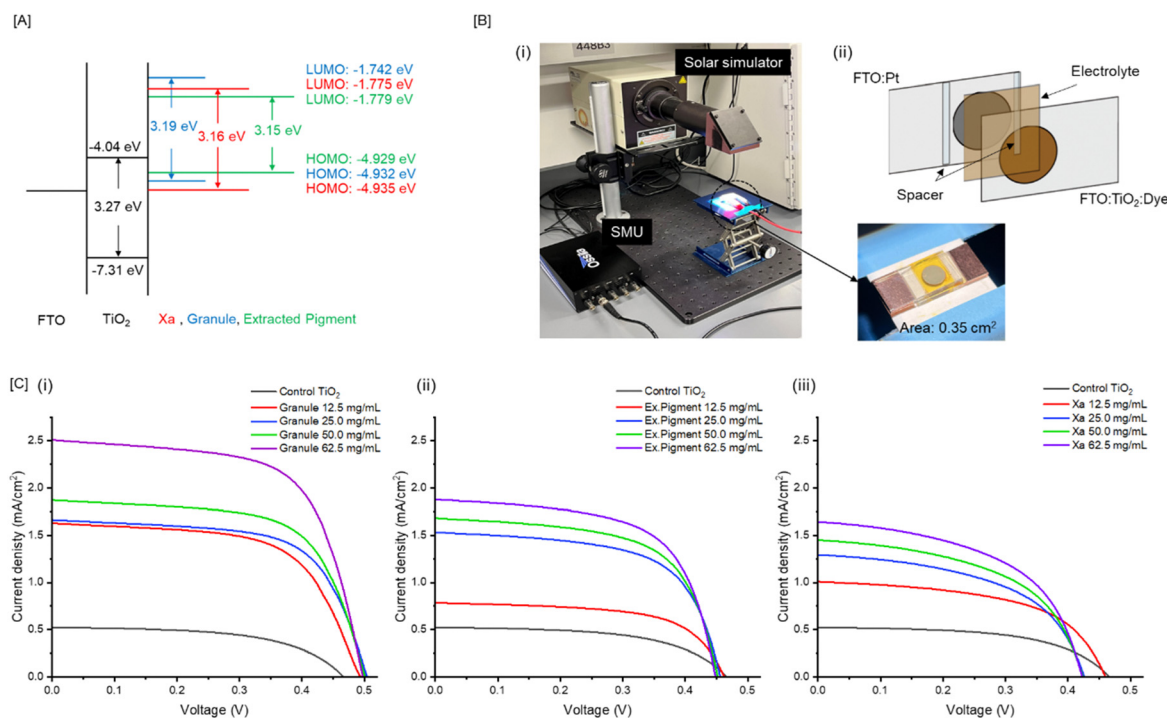

Fig. 2 Performance of the chromatophore-based materials incorporated within the modified DSSC. (A) Comparison of the energy band alignment of granules, extracted pigments, and synthetic Xa relative to the TiO$_2$ layer. (B) Overview of the assembled device and setup, where (i) is picture of the experimental framework and (ii) represents the assembled granule-based device (image and schematic). (C) Charts representing current density (*J*) *vs.* voltage (*V*) measurements acquired by the source measure unit (SMU) when each device is exposed to 100 mW cm^{-2} of solar simulated light. *J vs. V* curves are generated from DSSCs prepared at different loading concentrations for the (i) granule loaded cells, (ii) extracted pigment form granule loaded cells, and (iii) synthesized Xa loaded cells.

This journal is © The Royal Society of Chemistry 2025

J. Mater. Chem. C, 2025, **13**, 1138–1145 | **1141**

supporting the validity of our calculations. Based on our calculations, the granules, synthetic Xa, and extracted pigment all have relatively smaller bandgaps than the TiO$_2$, suggesting that solar illumination may be sufficiently energetic to drive the electron injection into the edge of the conduction band of TiO$_2$.[27]

Electrochemical analysis

To determine the energy levels of highest occupied molecular orbital (HOMO) and lowest unoccupied molecular orbital (LUMO) values, we next recorded cyclic voltammograms (CV) for each material. We observed reversible electrochemical behavior as expected,[28] with approximately the same peak oxidation and reduction currents across all materials (Fig. S3B, ESI†). The oxidation and reduction peaks are related to the electron and hole injection from conduction and valence bands. When taken together with the E_g determined from the absorption curves, we can use these values to estimate the HOMO and LUMO energies for the granules (−4.932 eV and −1.742 eV), pigment extracted from the granules (−4.932 eV and −1.779 eV), and synthetic Xa (−4.935 eV and −1.775 eV), respectively (Fig. 2A). These experimentally-derived values agreed well with previously calculated values estimated using density functional theory (DFT).[29]

Photovoltaic measurement

To understand the photosensitizing capacities of the granules, pigments extracted from the granules, and synthetic Xa, we varied the material loading density on each cell from 12.5 mg mL^{-1} to 62.5 mg mL^{-1}. In this range, we observed a corresponding increase in current density as a function of loading concentration, where the granule-based devices consistently performed better relative to the extracted pigment, synthetic Xa, and the control (Table 1). At concentrations above 62.5 mg mL^{-1}, we observed a decrease in photocurrent generation for the granule devices, suggesting a threshold concentration for performance.

Next, we analyzed the charge transfer, or photocurrent generation, after illuminating the constructed devices with 100 mW cm^{-2} light. Characteristic photovoltaic parameters like open circuit voltage (V_{OC}), short circuit current (J_{SC}), fill factor (FF), and photoconversion efficiency (η) were extrapolated from the generated current density (J) vs. voltage (V) curves (Fig. 2C). The control, non-photosensitized TiO$_2$ generated 0.46 ± 0.10 V, 0.52 ± 0.21 mA cm^{-2}, 55.87 ± 0.24%, and 0.14 ± 0.12% for V_{OC}, J_{SC}, FF, and η respectively. Application of 62.5 mg mL^{-1} of granules increased this photovoltaic performance to 0.498 ± 0.12 V, 2.51 ± 0.15 mA cm^{-2}, 64.03 ± 0.10%, 0.81 ± 0.14% for V_{OC}, J_{SC}, FF, and η. This ∼8× increase in photoconversion efficiency with the granules indicates that it can sufficiently collect and transfer photoexcited electrons to the conduction band of TiO$_2$. This feature was further investigated by reducing the illuminating light intensities from 100 to 75 mW cm^{-2} to assess the light sensitivities of the granules. We observed a decrease in photocurrent generation of 42.7% when light intensity was decreased from 100 to 75 mW cm^{-2} for the

Table 1 List of photovoltaic parameters of open circuit voltage (V_{OC}), short circuit current (J_{SC}), fill factor (FF) and photoconversion efficiency (η) based on collected J–V curves of TiO$_2$, granule, extracted pigment, and synthetic Xa at different loading concentrations

Sample	V_{OC} (V)	J_{SC} (mA cm^{-2})	FF (%)	η (%)
TiO$_2$				
	0.46 ± 0.10	0.52 ± 0.13	55.87 ± 0.24	0.14 ± 0.05
Granule				
12.5 mg mL^{-1}	0.49 ± 0.10	1.63 ± 0.05	61.31 ± 0.10	0.49 ± 0.02
25.0 mg mL^{-1}	0.50 ± 0.08	1.66 ± 0.15	63.96 ± 0.14	0.54 ± 0.08
50.0 mg mL^{-1}	0.50 ± 0.10	1.87 ± 0.21	63.99 ± 0.05	0.60 ± 0.15
62.5 mg mL^{-1}	0.50 ± 0.12	2.51 ± 0.15	64.03 ± 0.10	0.81 ± 0.14
Extracted pigment				
12.5 mg mL^{-1}	0.46 ± 0.06	0.78 ± 0.09	61.69 ± 0.02	0.22 ± 0.05
25.0 mg mL^{-1}	0.46 ± 0.04	1.53 ± 0.04	61.75 ± 0.15	0.43 ± 0.02
50.0 mg mL^{-1}	0.45 ± 0.05	1.68 ± 0.04	61.86 ± 0.05	0.47 ± 0.03
62.5 mg mL^{-1}	0.45 ± 0.15	1.88 ± 0.11	61.79 ± 0.12	0.52 ± 0.14
Xa				
12.5 mg mL^{-1}	0.46 ± 0.08	1.01 ± 0.05	54.86 ± 0.12	0.25 ± 0.07
25.0 mg mL^{-1}	0.43 ± 0.06	1.29 ± 0.12	51.92 ± 0.20	0.29 ± 0.08
50.0 mg mL^{-1}	0.42 ± 0.10	1.45 ± 0.04	55.02 ± 0.14	0.32 ± 0.07
62.5 mg mL^{-1}	0.42 ± 0.25	1.64 ± 0.12	52.14 ± 0.33	0.36 ± 0.11

granule loaded cells. This sensitivity was higher than the TiO$_2$ only cells, which exhibited a 30.8% decrease under these conditions (Fig. 3B). The enhanced photocurrent density appeared unique to the granule system especially when compared devices containing the extracted pigment and synthetic Xa. This is surprising considering Xa is the primary soluble portion of the granules.[7] Based on the UV-vis spectra, synthetic Xa demonstrated the highest visible absorption peak compared to the both the granules and the extracted pigment with the highest peak cathodic and anodic currents. As such, we originally anticipated that synthetic Xa would be the highest performer within these DSSCs. However, we observed the opposite; it was consistently the lowest performing material of all materials tested within the cells, with 0.423 ± 0.25 V, 1.64 ± 0.12 mA cm^{-2}, 52.14 ± 0.33%, 0.36 ± 0.11% for V_{OC}, J_{SC}, FF, and η, respectively at the 62.5 mg mL^{-1} condition. The extracted pigment cells performed better than the synthetic Xa cells, with photovoltaic performances of 0.448 ± 0.15 V, 1.88 ± 0.11 mA cm^{-2}, 61.79 ± 0.12%, and 0.52 ± 0.14% for V_{OC}, J_{SC}, FF, and η, respectively. Because the pigment extraction from the granules was a crude (i.e., unpurified) process, we believe other biological materials and proteins may also be part of the lysate and that these may facilitate photoconversion in the cells.

To investigate why the non-granular form of Xa consistently performed worse than the granules, we considered the performance of processed Xa from past reports. In our previous reports, we observed reversible color change of synthetic Xa when blended with TiO$_2$ in plasticized coatings.[24] Not surprisingly, we noted similar trends in our devices, where the color of the Xa loaded photoanode changed from brown (or dark yellow) to red (Fig. S4, ESI†). We also observed a light-induced color change in the extracted pigment devices; however, this process was slower (10 min vs. 1 min for the synthetic Xa, Fig. S4, ESI†). The slower reduction time of the extracted pigments, again, supported that they were more resistant to photoreduction than
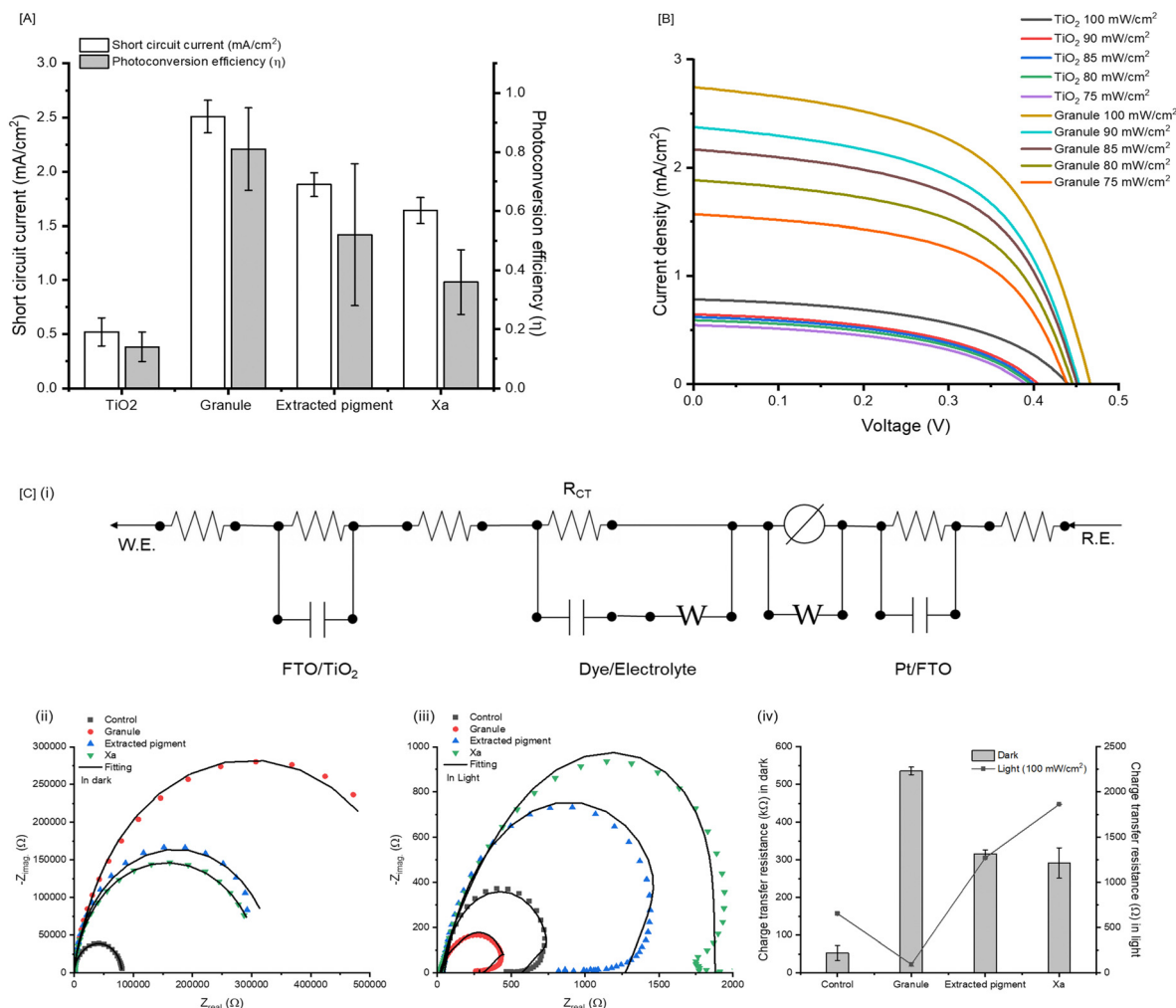
1142 | J. Mater. Chem. C, 2025, **13**, 1138–1145

This journal is © The Royal Society of Chemistry 2025

Fig. 3 Analysis of device performance for each material. (A) Representation of the photovoltaic parameters comparing short circuit current density (J_{SC}) and photoconversion efficiency (η) of TiO$_2$ at the maximum concentration (62.5 mg mL^{-1}) of granules, extracted pigment, and synthetic Xa loaded within the TiO$_2$ cells. (B) Demonstration of the light sensitivity of the granule only (62.5 mg mL^{-1}) devices compared to the control TiO$_2$, when light intensity is varied from 100 mW cm^{-2} to 75 mW cm^{-2}. (C) Analysis of the electrochemical impedance of the devices. This includes (i) the representative modified equivalent circuit used to extrapolate the electrochemical impedance spectroscopy (EIS) data for each material. Each material (62.5 mg mL^{-1}) was analyzed using EIS, where Nyquist plots were recorded under (ii) "dark" (*i.e.*, non-irradiated) and (iii) "light" illumination with 100 mW cm^{-2} light intensity conditions. (iv) Charge transfer resistance (R_{CT}) values under each condition were extrapolated for each device. Values represented as averages (N = 3 devices). Error is represented as standard deviation.

the synthetic form likely due to the non-specific granular materials (*i.e.*, proteins) co-extracted with the small molecules, which we know are present due to previous mass spectrometric reports.[8] While this light-activated color change cannot be decoupled from Xa performance, it poses a problem for photocurrent efficiency within DSSCs. Mainly, the photoreduction of Xa mitigates the efficient transfer of the photoexcited electrons to the semiconductor layer due to charge recombination within the cells. To better understand the differences in the charge transfer process, we used electrochemical impedance spectroscopy (EIS) for each cell approximated as the equivalent circuit presented in Fig. 3C. EIS experiments were recorded in the dark and under illuminated light (100 mW cm^{-2}), where we tracked changes in each material's impedance response across a range of frequencies to compare their electron-transport processes. In

the context of DSSCs, different frequency regions correspond to distinct electrochemical processes that are critical for device performance. The impedance response at high frequencies ($\sim 10\,000$ Hz) signifies charge transfer at the counter (Pt) electrode, while impedance at low frequencies (~ 0.01 Hz) reflects the Warburg impedance from the electrolyte. In DSSC applications, the intermediate frequency range reveals the recombination resistance (R_{CT}) across the TiO$_2$/dye/electrolyte interface,[30] where a lower R_{CT} leads to higher cell efficiency. Evaluation of EIS under dark conditions eliminates the contribution of photogenerated current, which resulted in a different electron distribution behavior compared to the impedance response after light illumination. Specifically, the granule loaded cell exhibited the lowest R_{CT} of 94.6 ± 20.1 Ω after light illumination. This reduction in R_{CT} facilitates improved current

This journal is © The Royal Society of Chemistry 2025

J. Mater. Chem. C, 2025, **13**, 1138–1145 | **1143**

flow, consequently enhancing the photovoltaic parameters. Pigment extracted from the granule displayed an R_{CT} values of 1274.3 ± 0.2 Ω, whereas synthesized Xa exhibited an R_{CT} values of 1866.5 ± 0.6 Ω. Furthermore, the distinct appearance of the tail in the low frequency region of synthetic Xa suggests a slower diffusion process of the electrolyte. Xa is a heterocyclic π-conjugated compound that is inherently redox active[28] (Fig. S5, ESI†). Redox activity can occur in some cases upon exposure of light.[24,29] This activity may contribute to the high charge-transfer resistance in our cells with Xa only. Consequently, Xa exhibits a higher charge recombination rate with slow electrolyte diffusion, resulting in lower cell performance compared to granules and extracted pigments. The differences in R_{CT} contribute to the differences in device performance. DSSCs require illumination of the photoanode, excitation of dye molecule, then subsequent injection of excited electrons into the conduction band of the TiO_2 semiconductor. In theory, these electrons travel through the external circuit to the counter electrode, where they reduce the electrolyte to, in turn, regenerate the oxidized dye molecules.[31] However, the inherent redox activity of Xa confounds this process due to its higher propensity to undergo charge-recombination, leading to an ultimately lower performing cell. The nanostructure enclosure afforded within the granules not only precludes charge recombination but also enables efficient photocurrent generation with the highest photoconversion efficiency of all conditions tested. Future studies will investigate the detailed molecular interactions within and outside the granules that enable these properties.

Conclusions

The hypothesis that pigment granules act as photosensitizers in the chromatophore to enable signal transduction was examined by applying the theoretical principles of DSSCs. By applying three different sensitizing species from similar biological origins, we have demonstrated that granules show enhanced photovoltaic parameters that are dependent on its loading concentration. While synthetic Xa and the extracted pigments from the granules also exhibit photovoltaic performances larger than the control, the soluble pigments undergo a spontaneous redox reaction with exposed light that leads to charge recombination with an ultimate consequence of lower photoconversion efficiency relative to the intact granules. This supports the conjecture that the granules themselves may be uniquely designed to create emergent optoelectronic properties in the chromatophore. Given these data together with the natural, dynamic features of the cephalopod chromatophores, we propose an additional path of light sensing/signaling that is not directly dependent on visual input. We propose that the granules within individual chromatophores may indirectly "sense" light to subsequently initiate photoconversion to electrons to transduce signal across the organ and to other adjacent organs in a new pathway that could potentially supplement, or in some cases bypass, the canonical ocular system. Future studies will be designed to investigate the compositional and structural origins of these fascinating functional properties with particular attention paid to the macromolecular makeup.

While our study only focused on the pigment granules (combinations of proteins and pigments[7,8]) as photosensitizers, future work will be designed to systematically explore other components in squid skin. These could include exploring the photosensitizing capacity of whole chromatophore cells, soluble metabolites, or even neighboring cells/organs which may possibly enhance, or in some cases inhibit, efficiency. For now, we highlight the first characterization of native granules as photosensitizers and describe a role for light sensing and signaling in the skin which has never been discussed for these incredible animals.

Author contributions

T. K. designed the overall experiments including fabrication, measurement, and data analysis. D. Q. B. contributed to extracting granules from the squid. L. F. D. contributed to lead the investigation and supervised the project. T. K. and L. F. D. prepared the manuscript and contributed to the discussion.

Data availability

The data supporting this article have been included within the manuscript and its additional files.

Conflicts of interest

The authors declare no competing financial interest.

Acknowledgements

References

1 A. Andouche, Y. Bassaglia, S. Baratte and L. Bonnaud, *Dev. Dyn.*, 2013, **242**, 560–571.

2 A. Chatterjee, B. Norton-Baker, L. E. Bagge, P. Patel and A. A. Gorodetsky, *Bioinspiration Biomimetics*, 2018, **13**, 045001.

3 L. M. Mäthger and R. T. Hanlon, *J. Cell Tissue Res.*, 2007, **329**, 179–186.

4 J. Yacob, A. C. Lewis, A. Gosling, D. H. J. S. Hilaire, L. Tesar, M. McRae and N. J. Tublitz, *J. Exp. Biol.*, 2011, **214**, 3423–3432.

1144 | *J. Mater. Chem. C*, 2025, **13**, 1138–1145

This journal is © The Royal Society of Chemistry 2025

5 B. U. Budelmann, *Mar. Freshwater Behav. Physiol.*, 1995, **25**, 13–33.

6 R. Hanlon, C.-C. Chiao, L. Mäthger, A. Barbosa, K. Buresch and C. Chubb, *Philos. Trans. R. Soc., B*, 2009, **364**, 429–437.

7 T. L. Williams, C. W. DiBona, S. R. Dinneen, S. F. Jones Labadie, F. Chu and L. F. Deravi, *Langmuir*, 2016, **32**, 3754–3759.

8 T. L. Williams, S. L. Senft, J. Yeo, F. J. Martín-Martínez, A. M. Kuzirian, C. A. Martin, C. W. DiBona, C.-T. Chen, S. R. Dinneen, H. T. Nguyen, C. M. Gomes, J. J. C. Rosenthal, M. D. MacManes, F. Chu, M. J. Buehler, R. T. Hanlon and L. F. Deravi, *Nat. Commun.*, 2019, **10**, 1004.

9 P. K. Loi and N. J. Tublitz, *Aquarium Sci. Conserv.*, 1998, **2**, 135–143.

10 A. C. Kingston, A. M. Kuzirian, R. T. Hanlon and T. W. Cronin, *J. Exp. Biol.*, 2015, **218**, 1596–1602.

11 L. M. Mäthger, N. Shashar and R. T. Hanlon, *J. Exp. Biol.*, 2009, **212**, 2133–2140.

12 B. Imarazene, A. Andouche, Y. Bassaglia, P.-J. Lopez and L. Bonnaud-Ponticelli, *Front. Physiol.*, 2017, **8**, 241427.

13 K. C. Buresch, K. M. Ulmer, D. Akkaynak, J. J. Allen, L. M. Mäthger, M. Nakamura and R. T. Hanlon, *J. Exp. Mar. Biol. Ecol.*, 2015, **462**, 121–126.

14 M. D. Ramirez and T. H. Oakley, *J. Exp. Biol.*, 2015, **218**, 1513–1520.

15 M. Suzuki, T. Kimura, H. Ogawa, K. Hotta and K. Oka, *PLoS One*, 2011, **6**, e18244.

16 T. Mirkovic, E. E. Ostroumov, J. M. Anna, R. Van Grondelle, G. Govindjee and G. D. Scholes, *Chem. Rev.*, 2017, **117**, 249–293.

17 A. C. N. Kingston, T. J. Wardill, R. T. Hanlon and T. W. Cronin, *PLoS One*, 2015, **10**, e0135381.

18 E. Rivera, D. Montemayor, M. Masia and D. F. Coker, *J. Phys. Chem. B*, 2013, **117**, 5510–5521.

19 M. Grätzel, *Nature*, 2001, **414**, 338–344.

20 A. Hagfeldt, G. Boschloo, L. Sun, L. Kloo and H. Pettersson, *Chem. Rev.*, 2010, **110**, 6595–6663.

21 J. Gong, K. Sumathy, Q. Qiao and Z. Zhou, *Renewable Sustainable Energy Rev.*, 2017, **68**, 234–246.

22 A. Bayat and E. Saievar-Iranizad, *J. Lumin.*, 2017, **192**, 180–183.

23 S. Hase, K. Wakamatsu, K. Fujimoto, A. Inaba, K. Kobayashi, M. Matsumoto, M. Hoshi and S. Negishi, *Pigm. Cell Res.*, 2006, **19**, 248–249.

24 C. L. Martin, K. R. Flynn, T. Kim, S. K. Nikolic, L. F. Deravi and D. J. Wilson, *Adv. Sci.*, 2023, **10**, 2302652.

25 P. Makuła, M. Pacia and W. Macyk, *J. Phys. Chem. Lett.*, 2018, **9**, 6814–6817.

26 K. M. Reddy, S. V. Manorama and A. R. Reddy, *Mater. Chem. Phys.*, 2003, **78**, 239–245.

27 J. Tao, T. Luttrell and M. Batzill, *Nat. Chem.*, 2011, **3**, 296–300.

28 A. Kumar, T. L. Williams, C. A. Martin, A. M. Figueroa-Navedo and L. F. Deravi, *ACS Appl. Mater. Interfaces*, 2018, **10**, 43177–43183.

29 D. J. Wilson, F. J. Martín-Martínez and L. F. Deravi, *ACS Sens.*, 2022, **7**, 523–533.

30 A. Omar, M. S. Ali and N. Abd Rahim, *Sol. Energy*, 2020, **207**, 1088–1121.

31 K. Zhu, S.-R. Jang and A. J. Frank, *J. Phys. Chem. Lett.*, 2011, **2**, 1070–1076.

This journal is © The Royal Society of Chemistry 2025

J. Mater. Chem. C, 2025, **13**, 1138–1145 | **1145**